

## MHD Mixed Convection Flow of casson Nanofluid over a Non-Linear Permeable Stretching Sheet in The Presence of Heat Generation or Absorption

G Kamala\*, Gangadhar K\*\*, M. V Ramanamurthy\*, P Suresh\*\*\*

\* Department of Mathematics & Computer Science, Osm,naia University, Hyderabad -7, Telangana, India,

\*\*Department of Mathematics, Acharya Nagarjuna University, Ongole, Andhra Pradesh -523001, India

\*\*\* Department of Mathematics & Hmanities, Chaitanya Bharathi Institute Of Technology, Hyderabad-75, Telangana, India.

---

**Abstract:** In this paper, numerical analysis has been carried out on the problem of magnetic hydro dynamic mixed convection flow of a Casson nanofluid past a nonlinear permeable stretching sheet with viscous dissipation in the presence of double stratification and heat generation or absorption. The governing partial differential equations were transformed into a system of ordinary differential equations using suitable similarity transformations. The resultant ordinary differential equations were then solved using Bvp4c mat lab solver. Effects of the physical parameters on the velocity, temperature and concentration profiles as well as the local skin friction coefficient, the heat and mass transfer rates are depicted in tabular form and discussed. The results indicate that the local Nusselt number decreases with an increase in both Brownian motion parameter ( $Nb$ ) and the thermophoresis parameter ( $Nt$ ). However the local Sherwood number ( $Sh$ ) increases with an increase in the parameter  $Nb$ . But it decreases as the values of  $Nt$  increases. Besides it was found that the surface temperature of a sheet increases with an increase in the heat generation ( $Q > 0$ ) or absorption parameter ( $Q < 0$ ). Comparison of present results with previous reported results has been found in excellent agreement.

**Keywords:** Nonlinear permeable stretching sheet, MHD, mixed convection, Casson nanofluid, double stratification.

---

### I. Introduction

The flow over a stretching sheet is relevant to several important engineering applications in the field of metallurgy and chemical engineering process. These applications involve the cooling of continuous strips or filaments by drawing them through a quiescent fluid. The steady two dimensional boundary layer flow of Newtonian fluid over a stretching surface has been studied by Crane. After this pioneering work the flow field over a stretching surface has drawn considerable attention and a good amount of literature has been generated on this problem. Javad and Sina (2012) investigated the effect of viscous dissipation on non liner stretching sheet and they concluded that the dimensionless temperature increases with increases in the nonlinear stretching parameter  $n$ . Mukhopadhaya (2013) studied the boundary layer flow over a porous non-linearly stretching sheet with partial slip at the boundary and he concluded that the rate of transport is considerably reduced with increasing values of non-linearly stretching parameter. Khan et al. (2014) investigated the three dimensional flow and heat transfer over a non-linearly stretching sheet. Khan and Hashim (2015) investigated the boundary layer flow and heat transfer to carreau fluid over a non linear stretching sheet and they concluded that on increasing the values of stretching parameter was to thin the momentum boundary layer thickness; however the opposite trend was noted for thermal boundary layer thickness. Vijayalakshmi and Shankar (2016) studied the effect of thermal radiation on boundary layer flow of viscous fluid over nonlinear stretching sheet with injection or suction.

Nanofluid is a new type of heat transfer fluid which contains a base fluid and nanoparticles. The term nanofluid is proposed by Choi (1995). The boundary layer flow and heat transfer over a permeable stretching sheet due to a nanofluid with the effect of magnetic field, slip boundary condition and thermal radiation have been investigated by Ibrahim and Shankar (2013) and they concluded that the local Nusselt number decreases with an increase in both Brownian motion parameter  $Nb$  and thermophoresis parameter  $Nt$ . However, the local Sherwood number increases with an increase in both thermophoresis parameter  $Nt$  and Lewis number  $Le$ , but it decreases as the values of  $Nb$  increase. Khan et al. (2014) studied the combined effects of Navier slip and magnetic field on boundary layer flow with heat and mass transfer of water-based nanofluid containing gyrotactic microorganisms over a vertical plate and they concluded that the magnetic field suppresses the dimensionless velocity and increases the dimensionless temperature inside the boundary layers. Lakshminarayana and Gangadhar (2014) concluded that the temperature and mass volume friction increases in the presence of thermophoresis parameter and the temperature increases and the mass volume friction decreases

in the presence of Brownian motion parameter. Zaimi et al. (2014) investigated the boundary layer flow and heat transfer over a non-linearly permeable stretching or shrinking sheet in a nanofluid. Mustafa et al. (2014) investigated the laminar two dimensional flow of nanofluid due to non-linearly stretching sheet with convective surface boundary condition. Das (2015) investigated the effect of partial slip on nanofluid flow over a non linear permeable stretching sheet and he concluded that an increase in the non linear stretching parameter  $n$  leads to increase the thermal boundary layer thickness and also nanoparticle concentration is an increasing function of each values of the nonlinear stretching parameter. Mabood et al. (2015) investigated the effect of viscous dissipation on a laminar boundary layer flow with heat and mass transfer of an electrically conducting water based nanofluid over a nonlinear stretching sheet and they concluded that the dimensionless velocity decreases and temperature increases with magnetic parameter and the thermal boundary layer thickness increases with Brownian motion and thermophoresis parameters.

In real life applications many materials like shampoos, printing ink, muds, condensed milk, paints, tomato paste, etc., show different characters which cannot be understood by Newtonian theory. So to describe such type of fluids it is necessary to introduce the non-Newtonian fluids. The fluid which does not obey Newton's law of viscosity is known as non-Newtonian fluid. All the properties of non-Newtonian fluid cannot be expressed in single non-Newtonian model; various models have been proposed in the literature and these models mainly categorized into three types namely differential, rate and integral type fluids. In the year of 1959, a model presented in the flow of viscoelastic fluid by Casson which was known as Casson fluid model. Casson fluid exhibits a yield stress. It is well known that Casson fluid is a shear thinning liquid which is assumed to have an infinite viscosity at zero rate of shear, a yield stress below which no flow occurs and a zero viscosity at an infinite rate of shear, i.e., if a shear stress less than the yield stress is applied to the fluid it behaves like a solid, whereas if a shear stress greater than yield stress is applied it starts to move. Fredrickson (1964) investigated the steady flow behavior of a Casson fluid in a tube. Mukhopadhaya et al. (2013) studied the Casson fluid flow over an unsteady stretching surface. They concluded that the effect of increased values of the Casson parameter is to suppress the velocity field. But the temperature is enhanced with increasing Casson parameter. Nadeem et al. (2013) studied MHD three dimensional Casson fluid flow past a porous linearly stretching sheet. Nadeem et al. (2014) studied the MHD three dimensional boundary layer flow of Casson nanofluid past a linearly stretching sheet with convective boundary condition and they concluded that the reduced Nusselt number is the decreasing function and the reduced Sherwood number is the function Brownian parameter  $N_b$  and thermophoresis parameter  $N_t$ . Isa et al. (2014) studied the mixed convection boundary layer flow of a Casson fluid near the stagnation point on a vertical surface when the wall is permeable, where there is suction or injection effect. Malik et al. (2014) studied the boundary layer flow of Casson non fluid over a vertical exponentially increasing cylinder. Bhattacharya et al. (2014) studied the boundary layer flow of Casson fluid over a permeable stretching or shrinking sheet. Hussanan et al. (2014) studied the unsteady boundary layer flow and heat transfer of a Casson fluid past an oscillating vertical plate with Newtonian heating and they concluded that the velocity decreases as Casson parameter increases and thermal boundary layer thickness increases with increasing Newtonian heating parameter. El-Dabe et al. (2015) studied the effect of MHD boundary layer flow of non-Newtonian Casson fluid on a moving edge with heat and mass transfer and induced magnetic field. Besthapu and Bandari (2015) studied the mixed convection MHD flow of a Casson nanofluid over a nonlinear permeable stretching sheet with viscous dissipation. Imran et al. (2016) investigated the slip effect on free convection flow of Casson fluid over an oscillating vertical plate. Khan and Khan (2016) studied the effect of MHD on boundary layer flow of a power-law nanofluid with new mass flux condition.

Stratification of fluid arises due to temperature variations, concentration differences, or the presence of different fluids. In practical situations where the heat and mass transfer mechanisms run parallel, it is interesting to analyze the effect of double stratification (stratification of medium with respect to thermal and concentration fields) on the convective transport in micropolar fluid. The analysis of free convection in a doubly stratified medium is a fundamentally interesting and important problem because of its broad range of engineering applications. These applications include heat rejection into the environment such as lakes, rivers, and seas; thermal energy storage systems such as solar ponds; and heat transfer from thermal sources such as the condensers of power plants. Although the effect of stratification of the medium on the heat removal process in a fluid is important, very little work has been reported in literature [Yang et al. (1972), Jaluria and Gebhart (1974), Jaluria and Himasekhar (1983), Angirasa and Peterson (1997)]. Srinivasacharaya and upender studied (2013) the effect of double stratification on MHD free convection in a micropolar fluid and they concluded that an increase in thermal (solutal) stratification parameter reduces the velocity, temperature (concentration), Skin friction coefficient; heat and mass transfer rate but enhance the concentration (temperature) and wall couple stress.

## II. Mathematical Formulation

Let us consider the two dimensional steady incompressible flow of a Casson nanofluid induced by a nonlinearly stretching sheet which is placed at  $y=0$ . The flow is confined to  $y > 0$ . By keeping the origin is fixed and sheet is stretched with nonlinear velocity  $u_w = ax^n$ , where  $n$  is nonlinear stretching parameter and  $>0$ ,  $x$  is the coordinate measured along the stretching surface. The nanofluid flows at  $y=0$ , where  $y$  is the coordinate normal to the surface. The fluid is electrically conducted due to an applied magnetic field  $B(x)$  normal to the stretching sheet. The magnetic Reynolds number is assumed small and so the induced magnetic field can be considered to be negligible. The surface is maintained at temperature  $T_w(x)$  and concentration  $C_w(x)$ . The temperature and the mass concentration of the ambient medium are assumed to be linearly stratified in the form  $T_\infty(x) = T_{\infty,0} + A_1x^2$  and  $C_\infty(x) = C_{\infty,0} + B_1x^2$  respectively, where  $A_1$  and  $B_1$  are constants and varied to alter the intensity of stratification in the medium and  $T_{\infty,0}$  and  $C_{\infty,0}$  are the beginning ambient temperature and nanoparticle volume fraction at  $x = 0$  respectively. The rheological equation of state for an isotropic flow of a Casson fluid (Eldabe and Salwa (1995)) can be expressed as

$$\tau_{ij} = \begin{cases} \left( \mu_B + \frac{p_y}{\sqrt{2\pi}} \right) 2e_{ij}, & \pi > \pi_c \\ \left( \mu_B + \frac{p_y}{\sqrt{2\pi_c}} \right) 2e_{ij}, & \pi < \pi_c \end{cases} \quad (2.1)$$

where  $\mu_B$  is plastic dynamic viscosity of the non-Newtonian fluid,  $p_y$  is the yield stress of fluid,  $\pi$  is the product of the component of deformation rate with itself, namely,  $\pi = e_{ij}e_{ij}$ ,  $e_{ij}$  is the  $(i, j)^{th}$  component of the deformation rate, and  $\pi_c$  is critical value of  $\pi$  based on non-Newtonian model.

With the usual Boussinesq and the boundary layer approximations, the governing equations of continuity, momentum, energy and spices are written as follows;

Continuity equation

$$\frac{\partial u}{\partial x} + \frac{\partial v}{\partial y} = 0 \quad (2.2)$$

Momentum equation

$$u \frac{\partial u}{\partial x} + v \frac{\partial u}{\partial y} = \nu \left( 1 + \frac{1}{\beta} \right) \frac{\partial^2 u}{\partial y^2} - \frac{\sigma B^2(x)}{\rho} u + g [\beta_T (T - T_\infty) + \beta_C (C - C_\infty)] \quad (2.3)$$

Energy equation

$$u \frac{\partial T}{\partial x} + v \frac{\partial T}{\partial y} = \alpha \frac{\partial^2 T}{\partial y^2} + \tau \left[ D_B \frac{\partial C}{\partial y} \frac{\partial T}{\partial y} + \frac{D_T}{T_\infty} \left( \frac{\partial T}{\partial y} \right)^2 \right] + \frac{\nu}{C_p} \left( 1 + \frac{1}{\beta} \right) \left( \frac{\partial u}{\partial y} \right)^2 + \frac{Q_0}{\rho C_p} (T_w - T_\infty) \quad (2.4)$$

Spices equation

$$u \frac{\partial C}{\partial x} + v \frac{\partial C}{\partial y} = D_B \frac{\partial^2 C}{\partial y^2} + \left( \frac{D_T}{T_\infty} \right) \frac{\partial^2 T}{\partial y^2} \quad (2.5)$$

The boundary conditions for the velocity, temperature and concentration fields are

$$\begin{aligned} y = 0 : u_w = ax^n, v = v_w, T = T_w, C = C_w \\ y = 0 : u = 0, v = 0, T = T_\infty, C = C_\infty. \end{aligned} \quad (2.6)$$

Where  $u$  and  $v$  are the velocity component along the  $x$  and  $y$  axes respectively,  $\alpha = \frac{k}{(\rho C)_f}$  is the thermal diffusivity,  $\nu$  is the kinematic viscosity,  $\mu$  is dynamic viscosity of the fluid,  $\kappa$  is vortex viscosity,  $\rho$  is fluid density,  $\beta$  is the Casson fluid parameter,  $\rho_f$  is the density of base fluid,  $g$  is the acceleration due to gravity,  $\beta_T$  is coefficient of thermal expansion,  $\beta_c$  is the coefficient of expansion with concentration,  $D_B$  is the Brownian diffusion coefficient,  $D_T$  is the thermophoresis diffusion coefficient,  $Q_0$  is the heat generation or absorption coefficient,  $\tau = \frac{(\rho C)_p}{(\rho C)_f}$  is the ratio of nanoparticle heat capacity and base fluid heat capacity,  $C$  is the volumetric volume coefficient,  $\rho_p$  is the density of the particles and  $c$  is the rescaled nanoparticle,  $k_p$  is the permeability of the porous medium,  $\sigma$  is the electrical conductivity,  $B_0$  is the magnetic field strength,  $c_p$  is the specific heat at constant pressure and  $m$  is the heat flux exponent. We assume that It is noted here that the case of uniform surface heat flux corresponds to  $m = 0$ .

The equation of continuity is satisfied for the choice of a stream function  $\psi(x, y)$  such that

$$u = \frac{\partial \psi}{\partial y} \quad \text{and} \quad v = -\frac{\partial \psi}{\partial x}$$

Now, we introduce the following similarity transformations

$$\eta = y \sqrt{\frac{a(n+1)}{2\nu}} x^{\frac{(n-1)}{2}}, \quad u = ax^n f'(\eta), \quad v = -\sqrt{\frac{av(n+1)}{2}} x^{\frac{(n-1)}{2}} \left[ f(\eta) + \frac{n-1}{n+1} \eta f'(\eta) \right] \quad (2.7)$$

The dimensionless temperature and concentration are

$$\theta(\eta) = \frac{T - T_{\infty,0}}{\Delta T} - \frac{A_1 x^2}{\Delta T}, \quad \Delta T = T_w(x) - T_{\infty,0} = M_1 x^2 \quad (2.8)$$

$$\phi(\eta) = \frac{C - C_{\infty,0}}{\Delta C} - \frac{B_1 x^2}{\Delta C}, \quad \Delta C = C_w(x) - C_{\infty,0} = N_1 x^2$$

and assume  $v_w = -\sqrt{\frac{av(n+1)}{2}} x^{\frac{(n-1)}{2}} f_w$ , where  $f_w$  is the suction or injection parameter.

After the substitution of these transformations (2.7) & (2.8) along with the equations (2.3) – (2.6) the resulting non-linear ordinary differential equations are written as follows:

$$\left(1 + \frac{1}{\beta}\right) f''' + ff'' - \frac{2}{n+1} (nf'^2 - Gr\theta - Gc\phi) - Mf' = 0 \quad (2.9)$$

$$\frac{1}{Pr} \theta'' + f\theta' + Nb\phi'\theta' + N_t \theta'^2 + Ec \left(1 + \frac{1}{\beta}\right) (f'')^2 + Q\theta - \varepsilon_1 f' = 0 \quad (2.10)$$

$$\phi'' + Le f\phi' + \frac{N_b}{N_b} \theta'' - \varepsilon_2 f' = 0 \quad (2.11)$$

The corresponding boundary conditions are

$$f(0) = f_w, \quad f'(0) = 1, \quad \theta(0) = 1 - \varepsilon_1, \quad \phi(0) = 1 - \varepsilon_2$$

$$f'(\infty) = 0, \quad \theta(\infty) = 0, \quad \phi(\infty) = 0 \quad (2.12)$$

Where prime denotes differentiation with respect to  $\eta$ . The Physical parameters involved in the above equations are defined as  $Pr = \frac{\nu}{\alpha}$  is Prandtl number.  $Le = \frac{\nu}{D_B}$  is Lewis number,

$N_b = \frac{D_B (C_w - C_\infty)(\rho C)_p}{\nu (\rho C)_f}$  is the Brownian motion parameter,  $N_t = \frac{D_T (T_w - T_\infty)(\rho C)_p}{\nu T_\infty (\rho C)_f}$  is the thermophoresis parameter,  $M = \frac{2\sigma B_0^2}{a\rho_f(n+1)}$  is magnetic parameter,  $Ec = \frac{u_w^2}{C_p(T_w - T_\infty)}$  is Eckert number,  $Gr = \frac{g\beta_T(T_w - T_\infty)}{a^2 x^{2n-1}}$  is called local Grashof number,  $Gc = \frac{g\beta_C(C_w - C_\infty)}{a^2 x^{2n-1}}$  is the local modified Grashof number,  $Q = \frac{Q_0}{\rho C_p a}$  is the heat generation (Q>0) or absorption (Q<0) parameter,  $\varepsilon_1 = \frac{x^2}{\Delta T} \frac{d}{dx} [T_\infty(x)]$  is the thermal stratification parameter and  $\varepsilon_2 = \frac{x^2}{\Delta C} \frac{d}{dx} [C_\infty(x)]$  is the solutal stratification parameter.

The quantities of the skin friction coefficient  $C_f$ , the local Nusselt number  $Nu_x$  and local Sherwood number  $Sh_x$  given as follows

$$C_f = \frac{\tau_w}{\rho u_w^2}$$

$$\text{where } \tau_w = \mu_B \left(1 + \frac{1}{\beta}\right) \left(\frac{\partial u}{\partial y}\right)_{y=0}, \quad Nu_x = \frac{xq_w}{k(T_w - T_\infty)}, \quad Sh_x = \frac{xq_m}{D_B(C_w - C_\infty)} \tag{2.13}$$

where k is the thermal conductivity of the nano fluid and  $q_w, q_m$  are the heat and mass fluxes at the surface respectively given by

$$q_w = -k \left(\frac{\partial T}{\partial y}\right)_{y=0}, \quad q_m = -D_B \left(\frac{\partial C}{\partial y}\right)_{y=0} \tag{2.14}$$

By substituting equation (2.7) & (2.8) into equations (2.13)-(2.14), we will get

$$Re_x^{1/2} C_f = \left(1 + \frac{1}{\beta}\right) f''(0), \quad Re_x^{-1/2} Nu_x = -\sqrt{\frac{n+1}{2}} \theta'(0), \quad Re_x^{-1/2} Sh_x = -\sqrt{\frac{n+1}{2}} \phi'(0)$$

where  $Re_x = \frac{u_w x}{\nu}$  and is known as local Reynolds number.

### III. Solution of the Problem

The system of ordinary differential equations (2.9)-(2.11) along with the boundary condition (2.12) are integrated numerically by first choosing initial guess values for  $f(0), f''(0), \theta'(0)$  and  $\phi'(0)$  to match the boundary conditions at  $\infty$ . Matlab bvp4c solver (ref. Shampine and Kierzenka (2000)) was used to integrate the system of equations. To verify the accuracy of the numerical results, we compared our results with those reported by Besthapu and Bandari (2015), Mahbood et al. (2015), Rana and Bhargava (2012) as shown in Table 1. The results are in very good agreement, thus lending confidence to the accuracy of the present results.

### IV. Results and Discussion

In order to acquire physical understanding, the velocity, temperature and concentration profiles have been discussed by varying the numerical values of the parameters encountered in the problem. The numerical results are tabulated and exhibited with graphical illustrations.

In order to discuss the effect of magnetic parameter (M), the other controlling parameters are taken as  $\beta = 0.5, n=2, Gr = 0.2, Gc = 0.2, Pr = 0.71, Nt = 0.2, Nb = 0.2, Ec = 0.5, Le = 2, f_w = 1.5, Q = 0.2, \varepsilon_1 = 0.1 \& \varepsilon_2 = 0.2$ . Figures 1(a), 1(b) and 1(c) shows that the effect of magnetic parameter (M) on dimensionless velocity, temperature and concentration profiles, respectively. It is obtained that the dimensionless velocity distribution decreases throughout the boundary layer with an increasing the magnetic parameter (see fig 1(a)).The Magnetic parameter is found to retard the velocity at all points of the flow field. It is because that the application of

transverse magnetic field will result in a resistive type force (Lorentz force) similar to drag force which tends to resist the fluid flow and thus reducing its velocity. Obviously, the magnetic parameter leads to an increase in dimensionless temperature and concentration throughout the entire boundary layer (see figs 1(b) & 1(c)).

Figures 2(a), 2(b) & 2(c) illustrate the effect of thermal Grashof number (Gr) on dimensionless velocity, temperature and concentration profiles. The other parameters are fixed as  $M=0.5$ ,  $\beta = 0.5$ ,  $n=2$ ,  $G_c = 0.2$ ,  $Pr = 0.71$ ,  $Nt = 0.2$ ,  $Nb = 0.2$ ,  $Ec = 0.5$ ,  $Le = 2$ ,  $f_w = 1.5$ ,  $Q = 0.2$ ,  $\varepsilon_1 = 0.1$  &  $\varepsilon_2 = 0.2$ . On increasing the thermal Grashof number, the dimensionless velocity significantly increased. Evidently, thickness of thermal and concentration boundary layers significantly decrease larger distance from the surface as the thermal Grashof number is increased.

The effect of solutal Grashof number ( $G_c$ ) on the dimensionless velocity, temperature and concentration fields are depicted in figures 3(a), 3(b) and 3(c) respectively. The other controlling parameters are set to be constant at  $M=0.5$ ,  $\beta = 0.5$ ,  $n=2$ ,  $Gr = 0.2$ ,  $Pr = 0.71$ ,  $Nt = 0.2$ ,  $Nb = 0.2$ ,  $Ec = 0.5$ ,  $Le = 2$ ,  $f_w = 1.5$ ,  $Q = 0.2$ ,  $\varepsilon_1 = 0.1$  &  $\varepsilon_2 = 0.2$ . It is observed that as the solutal Grashof number increases, the velocity remarkably increases. While the solutal Grashof number increases, the temperature and concentration distributions are decreased.

The other controlling parameters are set to be constant at  $M=0.5$ ,  $\beta = 0.5$ ,  $n=2$ ,  $Gr = 0.2$ ,  $G_c = 0.2$ ,  $Pr = 0.71$ ,  $Nt = 0.2$ ,  $Nb = 0.2$ ,  $Ec = 0.5$ ,  $Le = 2$ ,  $Q = 0.2$ ,  $\varepsilon_1 = 0.1$  &  $\varepsilon_2 = 0.2$ . Figures 4(a), 4(b) & 4(c) exemplifies the effect of suction or injection parameter ( $f_w$ ) on the dimensionless velocity, temperature and concentration distributions respectively. As depicted in figure 4(a), the velocity distribution is decreased by suction parameter ( $f_w > 0$ ) where as it is increased by injection parameter ( $f_w < 0$ ). It is obvious that imposed suction decreases the boundary layer thickness. In other words, imposed injection increases the velocity distribution in the boundary layer region. Thus it signifies that injection parameter helps the flow to penetrate more into the fluid. Figure 4(b) demonstrate the suction ( $f_w > 0$ ) decrease the temperature and injection ( $f_w < 0$ ) increase the temperature throughout the boundary layer. It can be viewed that suction will lead to fast cooling of the surface. This is remarkably important in numerous industrial applications. Further, it is noted that the surface receives heat due to injection parameter and from the surface for suction. Moreover, it is observed that the temperature increase near the surface due to injection and decreases until its value become zero at the outside of the boundary layer. Figure 4(c) demonstrates that suction parameter ( $f_w > 0$ ) decreases the concentration distribution where as injection parameter increases it.

Figures 5(a), 5(b) & 5(c) describe the effect of non-Newtonian Casson fluid parameter ( $\beta$ ) on the dimensionless velocity, temperature and concentration profiles. The other controlling parameters are set to be constant at  $M=0.5$ ,  $n=2$ ,  $Gr = 0.2$ ,  $G_c = 0.2$ ,  $Pr = 0.71$ ,  $Nt = 0.2$ ,  $Nb = 0.2$ ,  $Ec = 0.5$ ,  $Le = 2$ ,  $f_w = 1.5$ ,  $Q = 0.2$ ,  $\varepsilon_1 = 0.1$  &  $\varepsilon_2 = 0.2$ . It is observed that the dimensionless velocity in the boundary layer decrease with the increase of Casson fluid parameter. When Casson fluid parameter increases, the temperature and concentration distributions in the boundary layer region are increased. The findings are similar to that of Mukhopadhyay (2013).

The phenomenon in which the particles can diffuse under the effect of a temperature gradient is called thermophoresis. The influence thermophoresis parameter ( $Nt$ ) on dimensionless temperature and concentration profiles can be viewed in figures 6(a) & 6(b) respectively. The other controlling parameters are set to be constant at  $M=0.5$ ,  $\beta = 0.5$ ,  $n=2$ ,  $Gr = 0.2$ ,  $G_c = 0.2$ ,  $Pr = 0.71$ ,  $Nb = 0.2$ ,  $Ec = 0.5$ ,  $Le = 2$ ,  $f_w = 1.5$ ,  $Q = 0.2$ ,  $\varepsilon_1 = 0.1$  &  $\varepsilon_2 = 0.2$ . On increasing the thermophoresis parameter, physically, imply high temperature gradients. As far as the concentration profile is considered, the concentration distribution increases away from the surface with the increase in thermophoresis parameter.

The random motion of nanoparticles within the base fluid is called Brownian motion which occurs due to the continuous collisions between the nanoparticles and molecules of the base fluid. Figures 7(a) and 7(b) shows the effects on velocity, temperature and nanoparticle volume fraction profiles for various values of Brownian motion parameter ( $Nb$ ). The effect of Brownian motion parameter  $Nb$  are explicated by setting the values of other parameters to be constant at  $M=0.5$ ,  $\beta = 0.5$ ,  $n=2$ ,  $Gr = 0.2$ ,  $G_c = 0.2$ ,  $Pr = 0.71$ ,  $Nt = 0.2$ ,  $Ec = 0.5$ ,  $Le = 2$ ,  $f_w = 1.5$ ,  $Q = 0.2$ ,  $\varepsilon_1 = 0.1$  &  $\varepsilon_2 = 0.2$ . It is noticed that temperature profiles are increased when Brownian motion parameter  $Nb$  increases. The physics behind the rise in temperature is that the increased Brownian motion parameter increases the thickness of the thermal boundary layer. However, in the case of nanoparticle volume fraction, it results in a decrease while Brownian motion parameter is increased away from the surface.

In order to discuss the influence of thermal stratification parameter ( $\varepsilon_1$ ), the other parameters are set constantly at  $M=0.5$ ,  $\beta = 0.5$ ,  $n=2$ ,  $Gr = 0.2$ ,  $G_c = 0.2$ ,  $Pr = 0.71$ ,  $Nt = 0.2$ ,  $Nb = 0.2$ ,  $Ec = 0.5$ ,  $Le = 2$ ,  $f_w = 1.5$ ,  $Q = 0.2$  &  $\varepsilon_2 = 0.2$ . From figures 8(a) and 8(b), it is noted that on increasing thermal stratification parameter, the thermal and concentration boundary layers decreases. From this, it is evidently seen that the thermal stratification tends to delay the thermal boundary layer flow process. Moreover, it will have some practical implications on the heat transfer amplification process.

The other parameters are set as  $M=0.5$ ,  $\beta = 0.5$ ,  $n=2$ ,  $Gr = 0.2$ ,  $Gc = 0.2$ ,  $Pr = 0.71$ ,  $Nt = 0.2$ ,  $Nb = 0.2$ ,  $Le = 2$ ,  $f_w = 1.5$ ,  $Q = 0.2$ ,  $\varepsilon_1 = 0.1$  &  $\varepsilon_2 = 0.2$ . The influence of Eckert number ( $Ec$ ) on the temperature profiles within the boundary layer region is shown in the figure 9. As compared to the case of absence of viscous dissipation, it is understood that the temperature profile is increased on increasing the Eckert number. Due to viscous heating, the increase in the fluid temperature is enhanced and appreciable for higher values of Eckert number. In other words, increasing the Eckert number leads to a coolness of the wall. Consequently, a heat transfer of heat to the fluid occurs, which causes a rise in the temperature of a fluid.

The effect of heat generation ( $Q>0$ ) or absorption ( $Q<0$ ) parameter and the temperature profiles are exhibited in figure 10. The other controlling parameters are set to be constant as  $M=0.5$ ,  $\beta = 0.5$ ,  $n=2$ ,  $Gr = 0.2$ ,  $Gc = 0.2$ ,  $Pr = 0.71$ ,  $Nt = 0.2$ ,  $Nb = 0.2$ ,  $Ec = 0.5$ ,  $Le = 2$ ,  $f_w = 1.5$ ,  $\varepsilon_1 = 0.1$  &  $\varepsilon_2 = 0.2$ . It can be observed that the effect of heat absorption results in a fall of temperature since heat resulting from the wall is observed. Obviously, the heat generation leads to an increase in temperature throughout the entire boundary layer. Furthermore, it should be noted that for the case of heat generation, the fluid temperature becomes maximum in the fluid layer adjacent to the wall rather at the wall. In fact, the heat generation effect not only has the tendency to increase the fluid temperature but also increases the thermal boundary layer thickness. Due to heat absorption, it is observed that the fluid temperature as well as the thermal boundary layer thickness is decreased. No significance in heat distribution is observed among the fluids in the presence of heat absorption.

The other parameters are set as  $M=0.5$ ,  $\beta = 0.5$ ,  $n=2$ ,  $Gr = 0.2$ ,  $Gc = 0.2$ ,  $Nt = 0.2$ ,  $Nb = 0.2$ ,  $Ec = 0.5$ ,  $Le = 2$ ,  $f_w = 1.5$ ,  $Q = 0.2$ ,  $\varepsilon_1 = 0.1$  &  $\varepsilon_2 = 0.2$ . The effect of Prandtl number ( $Pr$ ) on temperature profiles is illustrated in figure 11. It can be observed that the temperature profile is decreased on increasing Prandtl number. The ratio between momentum diffusivity and thermal diffusivity of the fluid is known as Prandtl number. Physically, increasing Prandtl number becomes a key factor to reduce the thickness of the thermal boundary layer.

Setting the other parameters to be constant as  $M=0.5$ ,  $\beta = 0.5$ ,  $n=2$ ,  $Gr = 0.2$ ,  $Gc = 0.2$ ,  $Pr = 0.71$ ,  $Nt = 0.2$ ,  $Nb = 0.2$ ,  $Ec = 0.5$ ,  $Le = 2$ ,  $f_w = 1.5$ ,  $Q = 0.2$ ,  $\varepsilon_1 = 0.1$ . The discussion is now made only by varying the solutal stratification parameter ( $\varepsilon_2$ ). The effect for the variation of solutal stratification parameter on the concentration profile is exemplified in figure 12. It is confirmed that the concentration distribution is significantly decreased while the values of solutal stratification parameter is increased.

Table 2 shows that the Skin friction coefficient, Local Nusselt number and Local Sherwood number (which are respectively proportional to  $\left[ -\left(1 + \frac{1}{\beta}\right) f''(0), -\sqrt{\frac{n+1}{2}} \theta'(0) \text{ \& } -\sqrt{\frac{n+1}{2}} \phi'(0) \right]$  for different values of

Casson fluid parameter, non-linear stretching parameter, thermal Grashof number, solutal Grashof number, magnetic parameter, Prandtl number, thermophoresis parameter, Brownian motion parameter and suction or injection parameter respectively. Increasing the Casson fluid parameter or thermal Grashof number or solutal Grashof number strictly decreases the value of both skin friction coefficient and local Sherwood number while local Nusselt number increases. The skin friction coefficient, local Nusselt number and local Sherwood numbers are significantly decreased by increasing the non linear stretching parameter and suction or injection parameter. On increasing the Brownian motion parameter or magnetic parameter strictly increases the values of both skin friction coefficient and local Sherwood number where as local Nusselt number decreased. Moreover, the local Nusselt number and local skin friction coefficient are increased on increasing the Prandtl number while the local Sherwood number decreased. This signifies that a fluid with larger  $Pr$  possess larger heat capacity and hence improves the heat transfer. On the other hand, the skin friction coefficient, local Nusselt number and local Sherwood number are decreased by increasing the thermophoresis parameter.

Table 3 illustrates that the effect of viscous dissipation, Lewis number, heat generation or absorption parameter, thermal stratification parameter and solutal stratification parameter on the local skin friction coefficient, local Nusselt number and local Sherwood number. It is observed that increasing Eckert number or heat generation or absorption parameter significantly decreases the skin friction coefficient and rate of heat transfer whereas rate of mass transfer is increased. On increasing the Lewis number, slight decrease in the rate of heat transfer and slight increase in skin friction coefficient and mass transfer rate are observed. When thermal stratification number is increased, skin friction coefficient is significantly increased and a decrease in the rate of heat and mass transfer can be noticed. The skin friction coefficient heat transfer rate is increased but mass transfer rate decreased on increasing the solutal stratification parameter.

## V. Conclusion

In this chapter, a numerical investigation has been carried out to discuss the double stratification and heat generation or absorption effects on magneto hydrodynamic mixed convection flow of a Casson nanofluid over a nonlinear permeable stretching sheet under the influence of viscous dissipation. The concluding facts for the present work after a thorough observation are briefed as follows

1. On increasing magnetic parameter or Casson fluid parameter and simultaneously decreasing buoyancy parameters (Gr, Gc) in a significant decrease of the momentum boundary layer thickness whereas the thermal and concentration boundary layer thickness increases of the fluid.
2. Thickness of the thermal and concentration boundary layers significantly increases away from the surface where the thermophoresis parameter increases.
3. When the Brownian motion parameter increases, the thermal boundary layer thickness increases where as concentration boundary layer thickness decreases.
4. On increasing thermal stratification parameter results in significant decrease of the thermal and concentration boundary layer thickness.
5. From low thermal stratification to high thermal stratification, Skin friction coefficient increases whereas local Nusselt and Sherwood number increased.
6. From low solutal stratification parameter to high solutal stratification parameter, the skin coefficient and local Nusselt number are increased whereas mass transfer rate decreased.

**Table 1** Comparison of  $-\theta'(0)$  and  $-\phi'(0)$  with the available results in literature for different values of  $n$  when  $Pr = 0.7, Le = 2, Nt = Nb = 0.5, Ec = Q = M = fw = Gr = Gc = \epsilon_1 = \epsilon_2 = 0, \beta \rightarrow \infty$ .

n	$-\theta'(0)$				$-\phi'(0)$			
	Present study	Besthapu and Bandari (2015)	Mabood et al. (2015)	Rana & Bhargava (2012)	Present study	Besthapu and Bandari (2015)	Mabood et al. (2015)	Rana & Bhargava (2012)
0.2	0.325221	0.3296	0.3295	0.3299	0.805682	0.8135	0.8134	0.8132
0.3	0.321608	0.3262	0.3262	0.3216	0.798441	0.8068	0.8067	0.7965
3.0	0.297992	0.3050	0.3050	0.3053	0.750777	0.7633	0.7633	0.7630
10.0	0.292190	0.2999	0.2999	0.3002	0.738961	0.7527	0.7527	0.7524
20.0	0.290697	0.2986	0.2986	0.2825	0.735912	0.7500	0.7500	1.4548

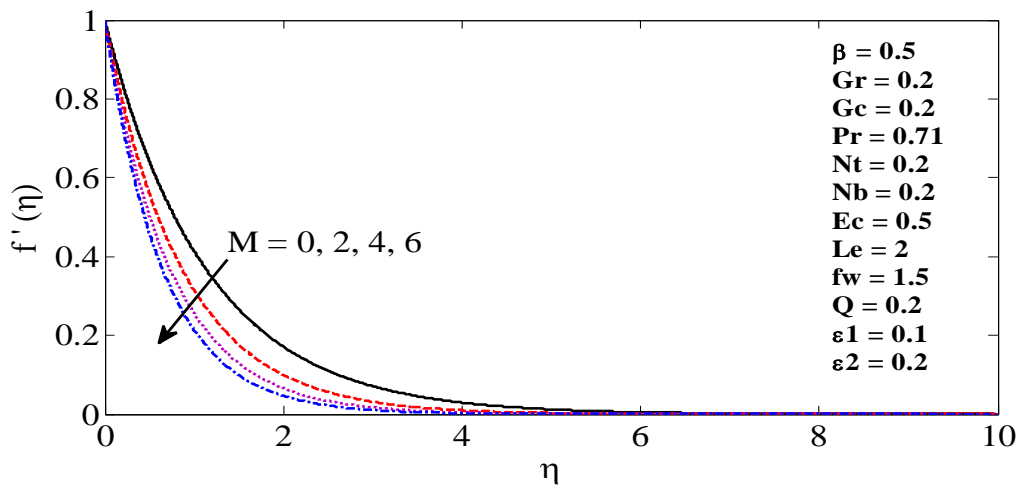


**Figure 1(a)** Velocity profiles for different values of M

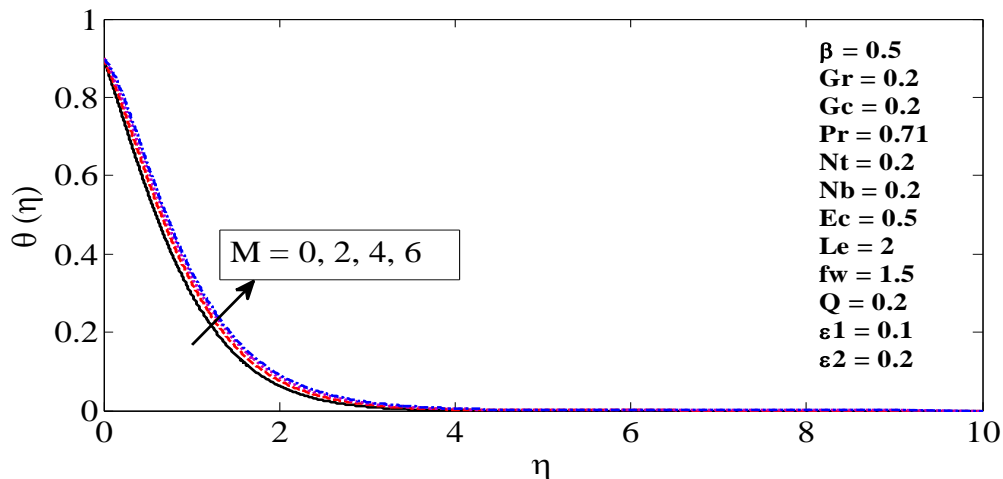


**Figure 1(b)** Temperature profiles for different values of M

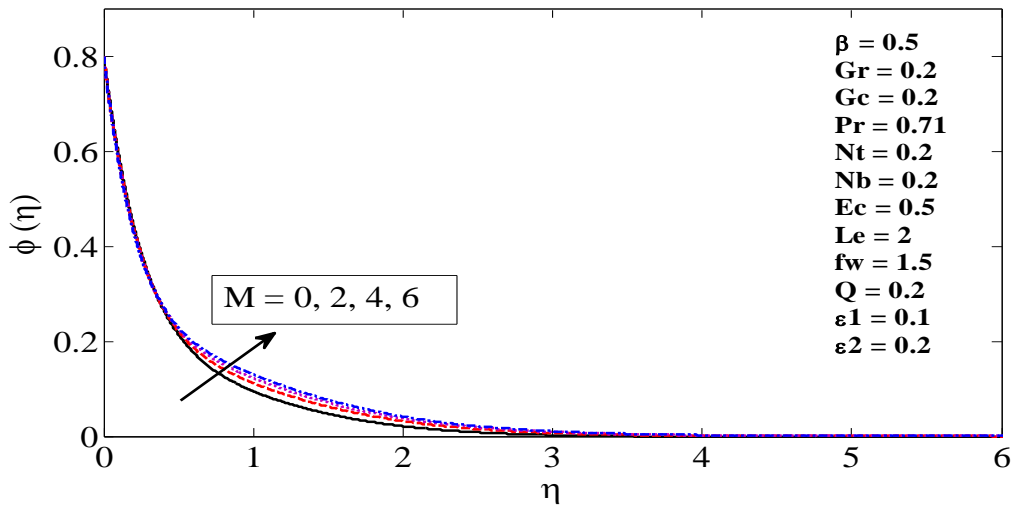


Figure 1(c) Concentration profiles for different values of  $M$

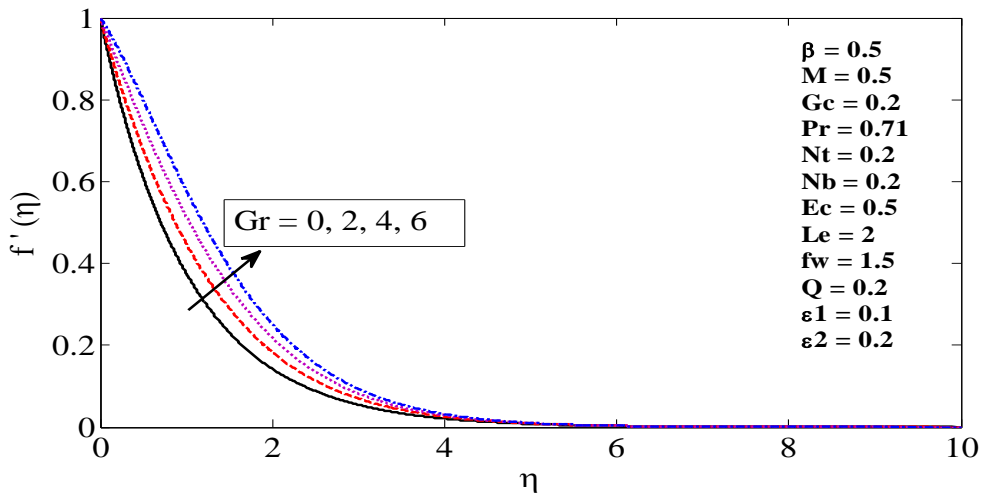


Figure 2(a) Velocity profiles for different values of  $Gr$

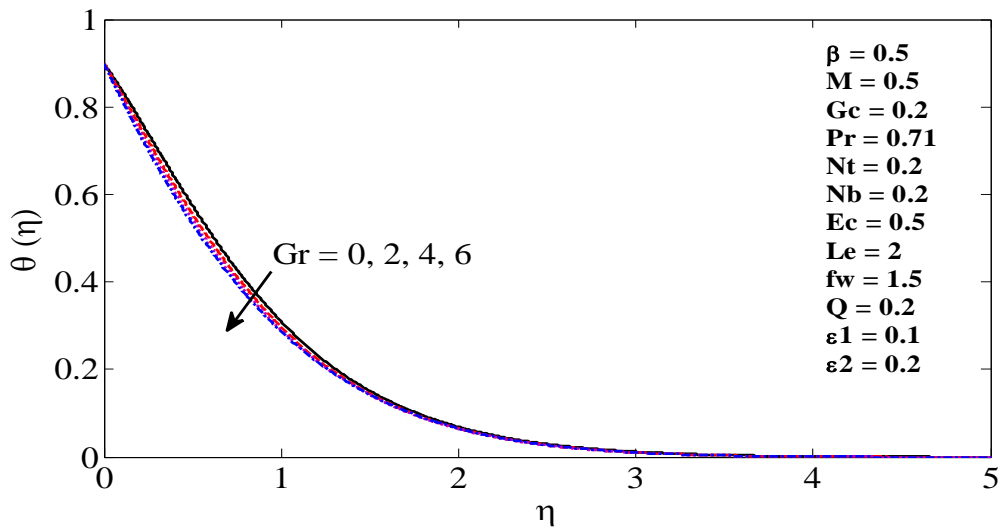


Figure 2(b) Temperature profiles for different values of  $Gr$

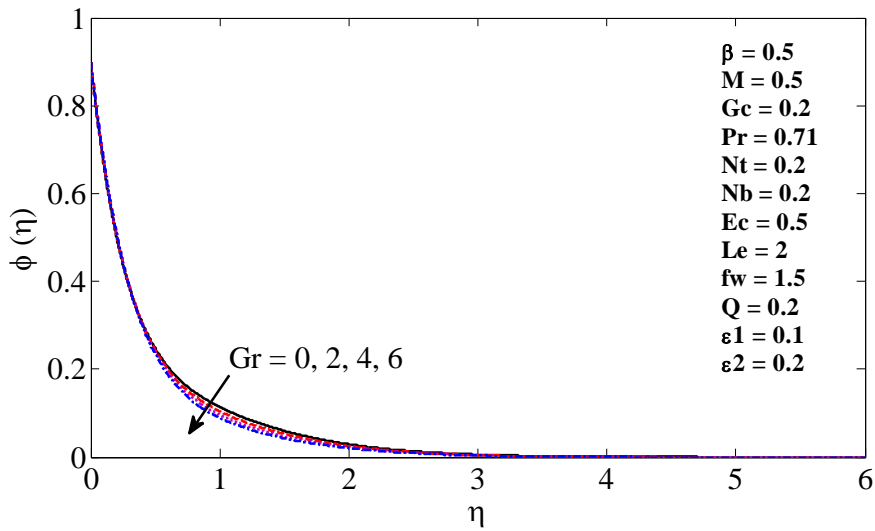


Figure 2(c) Concentration profiles for different values of  $Gr$

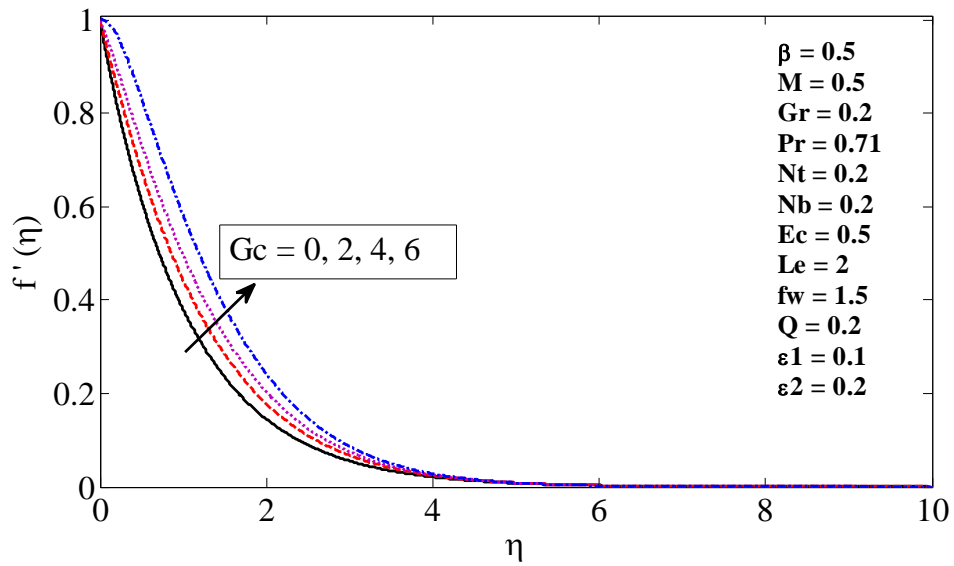


Figure 3(a) Velocity profiles for different values of  $Gc$

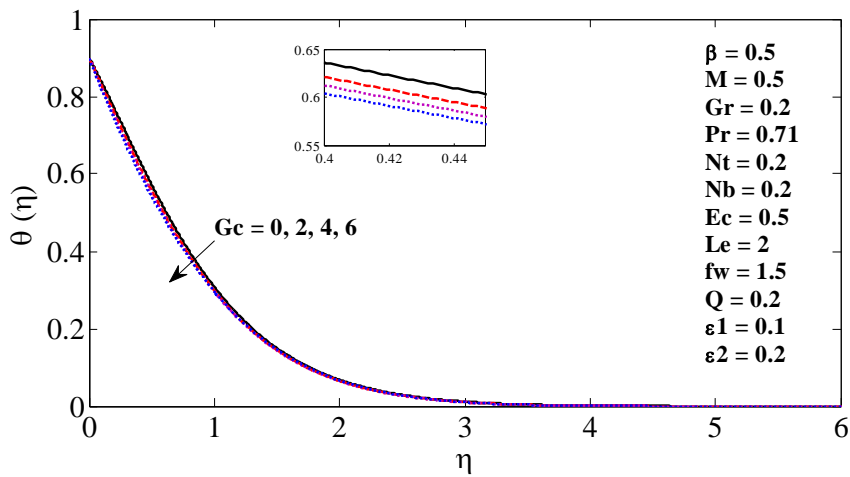


Figure 3(b) Temperature profiles for different values of  $Gc$

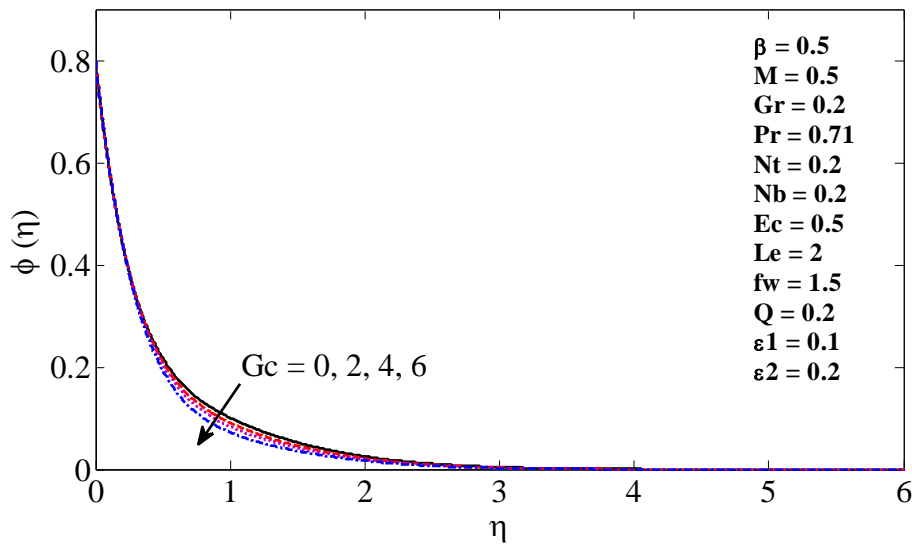


Figure 3(c) Concentration profiles for different values of  $G_c$

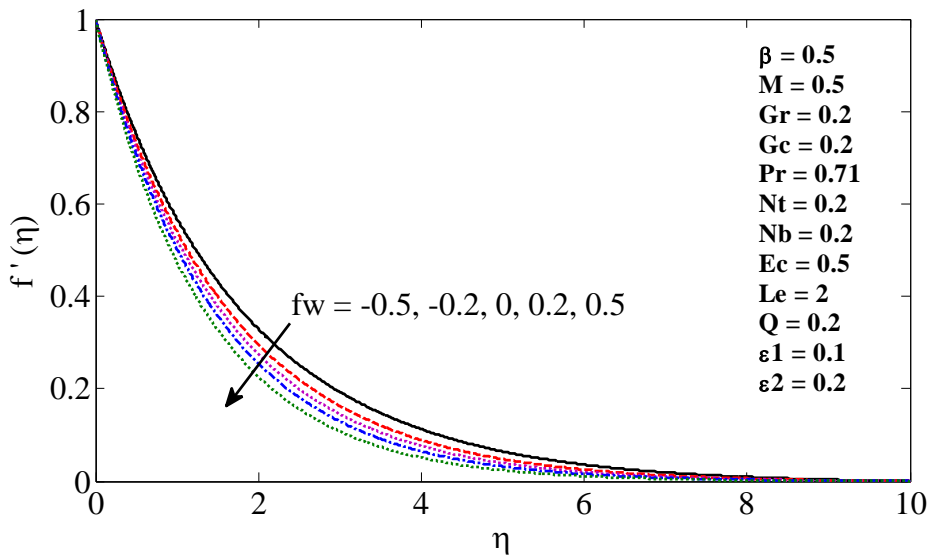


Figure 4(a) Velocity profiles for different values of  $f_w$

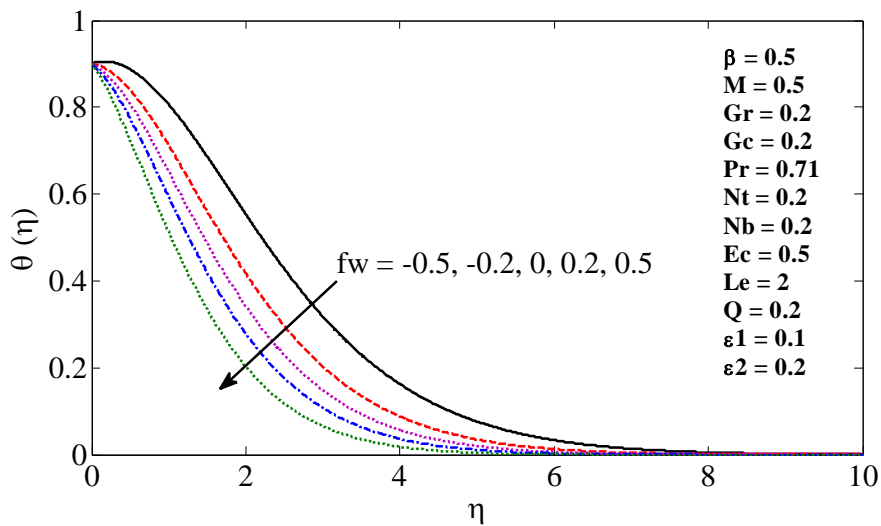


Figure 4(b) Temperature profiles for different values of  $f_w$

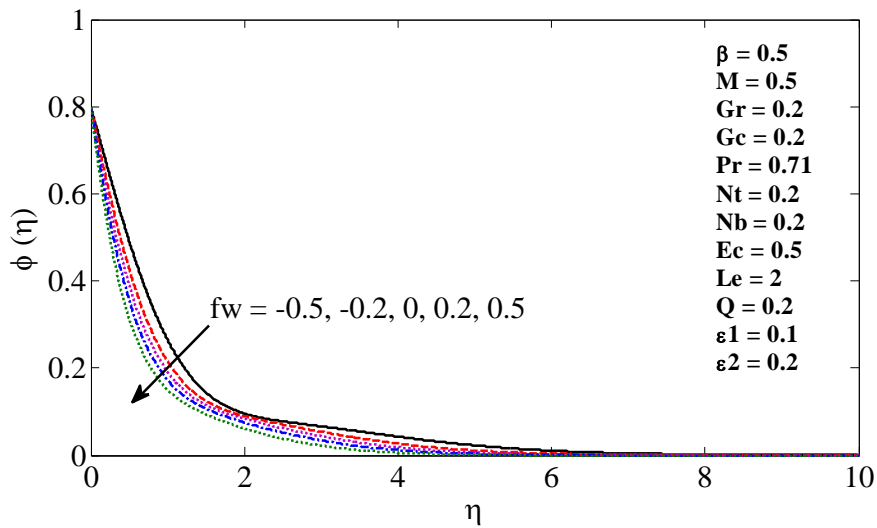


Figure 4(c) Concentration profiles for different values of  $f_w$

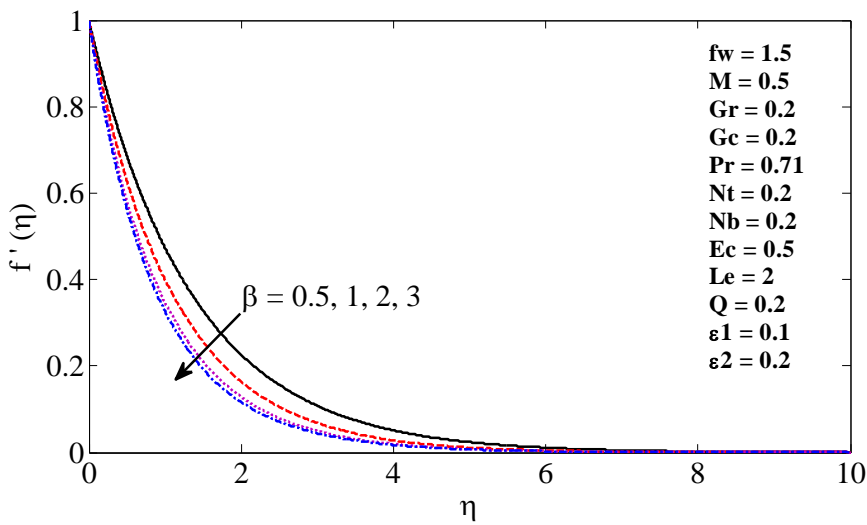


Figure 5(a) Velocity profiles for different values of  $\beta$

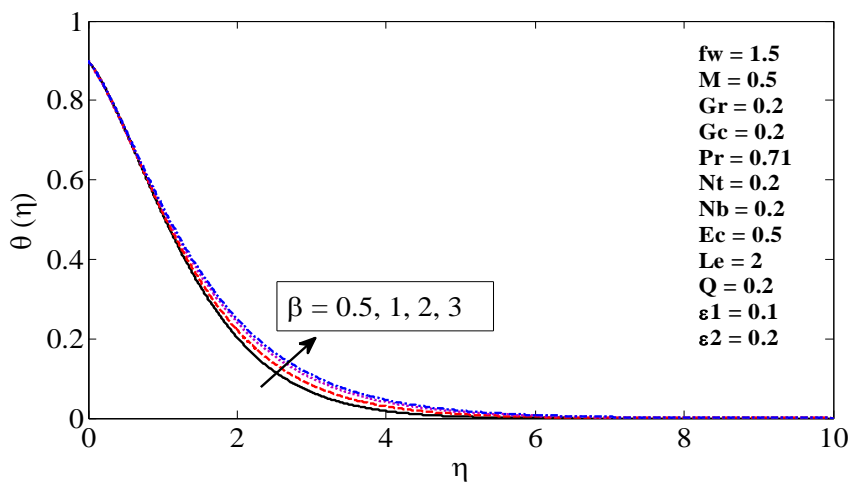


Figure 5(b) Temperature profiles for different values of  $\beta$

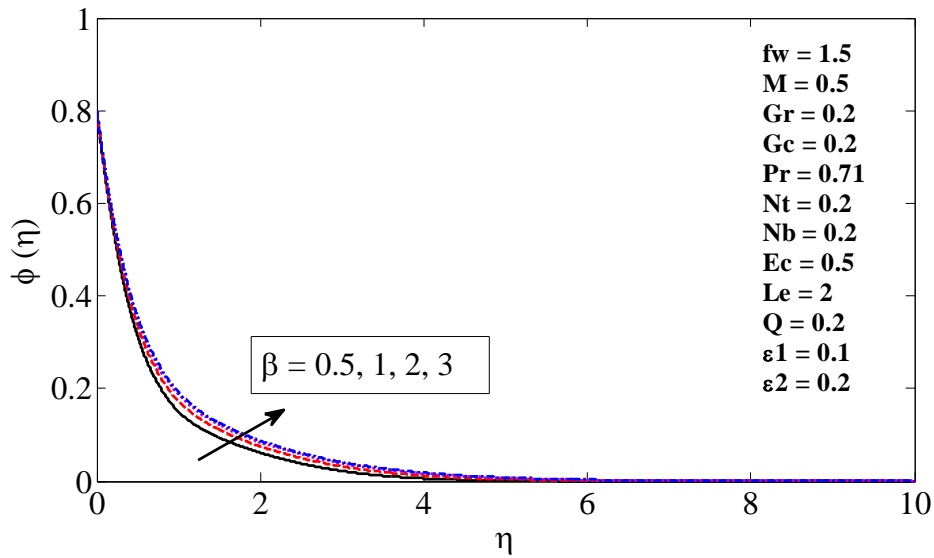


Figure 5(c) Concentration profiles for different values of  $\beta$

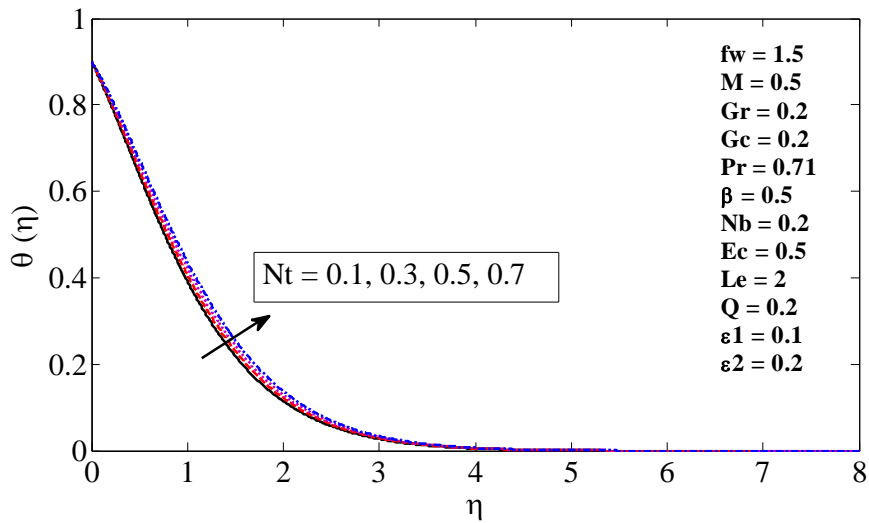


Figure 6(a) Temperature profiles for different values of  $Nt$

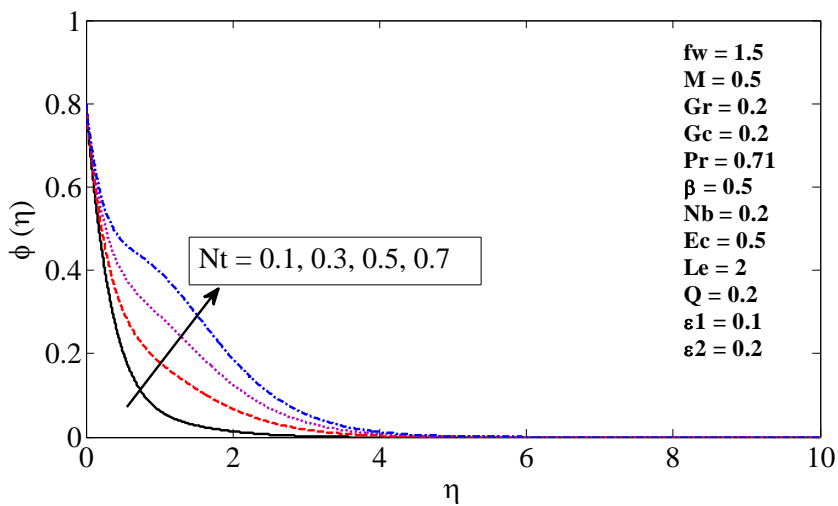


Figure 6(b) Concentration profiles for different values of  $Nt$

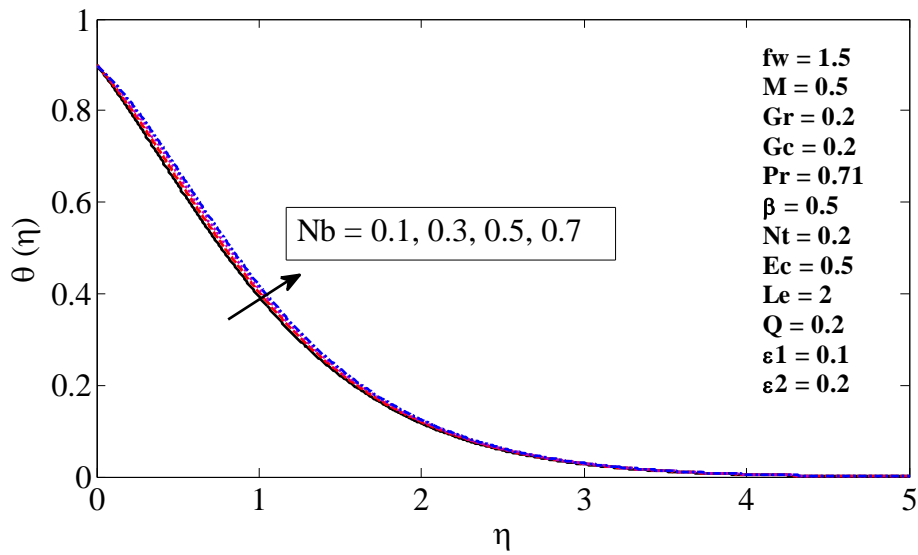


Figure 7(a) Temperature profiles for different values of  $Nb$

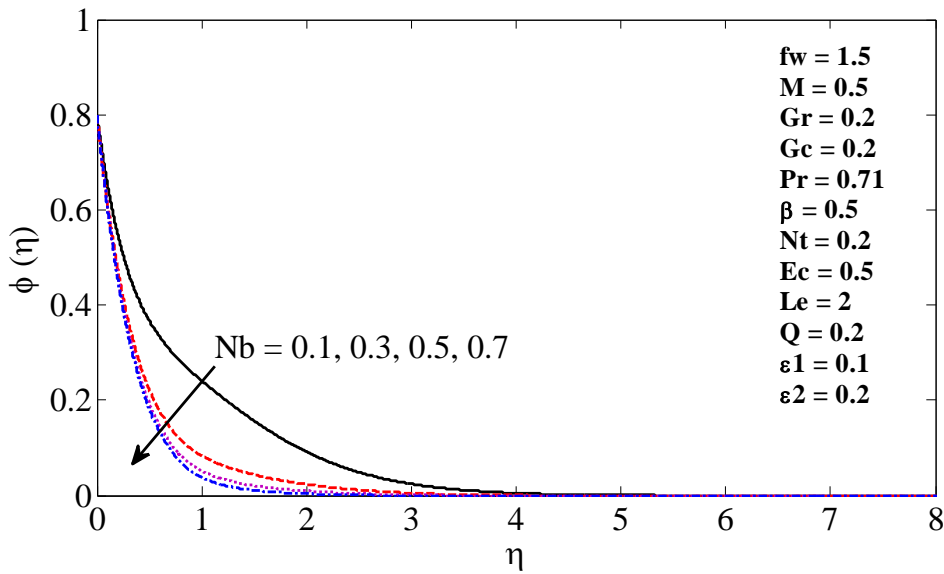


Figure 7(b) Concentration profiles for different values of  $Nb$

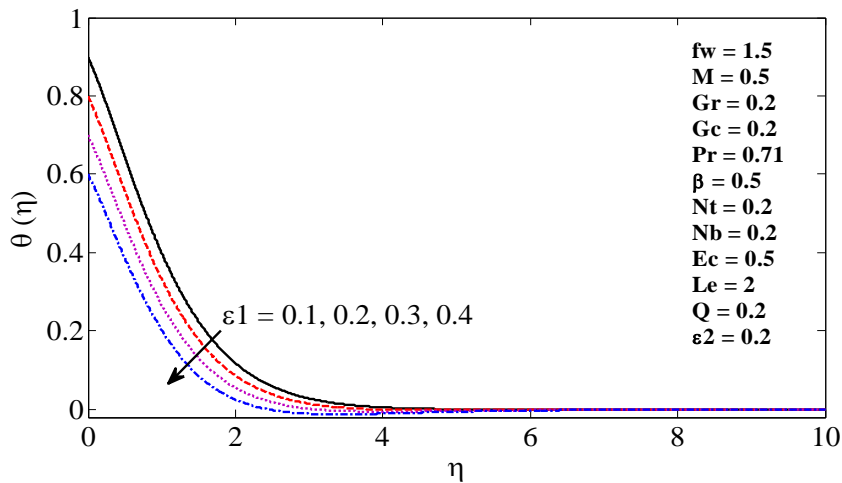


Figure 8(a) Temperature profiles for different values of  $\epsilon_1$

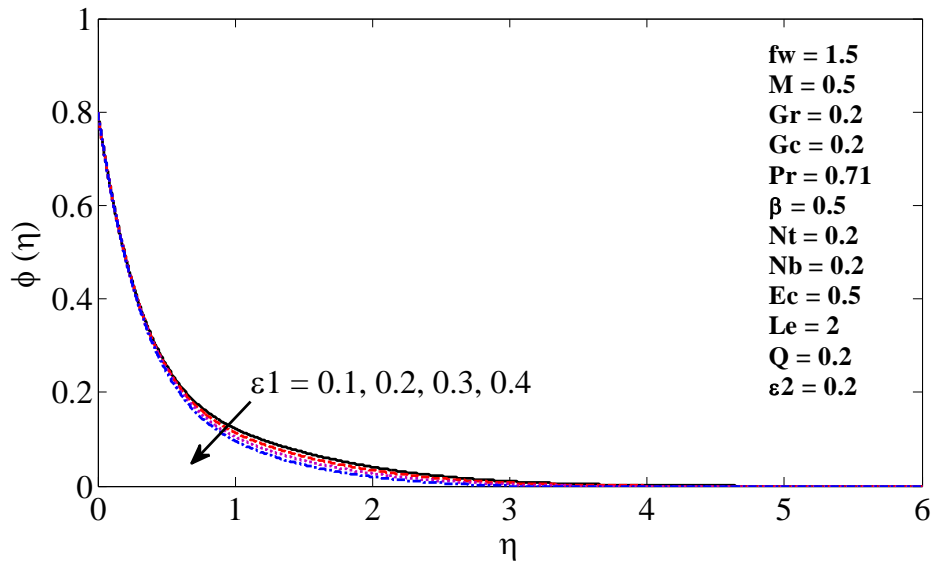


Figure 8(b) Concentration profiles for different values of  $\varepsilon_1$

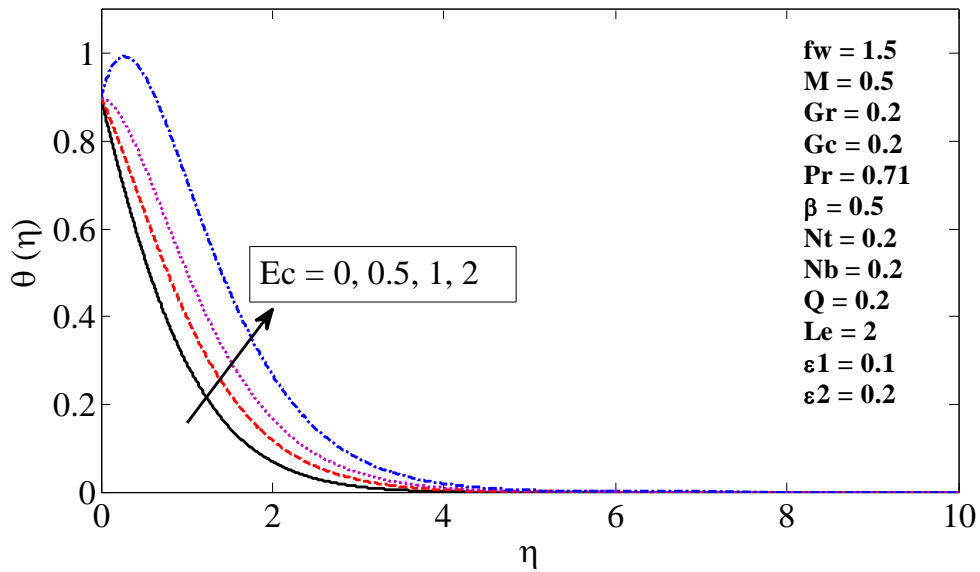


Figure 9 Temperature profiles for different values of  $Ec$

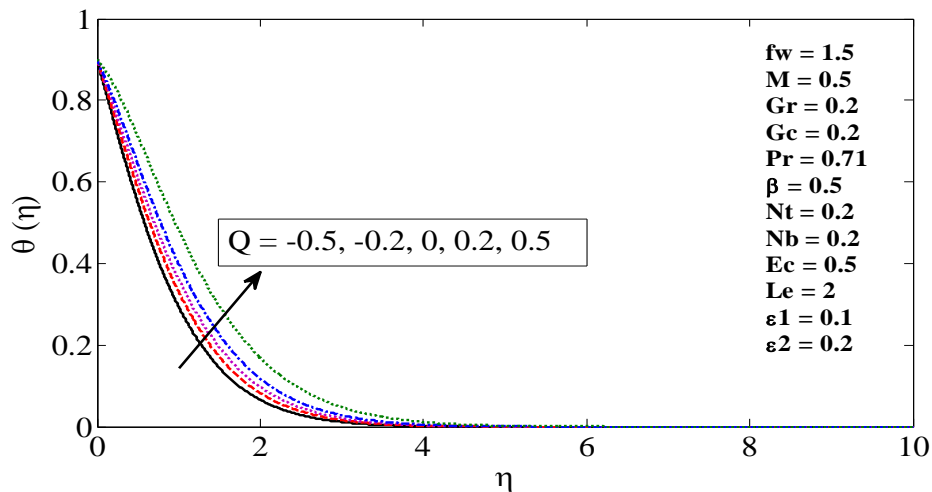


Figure 10 Temperature profiles for different values of  $Q$

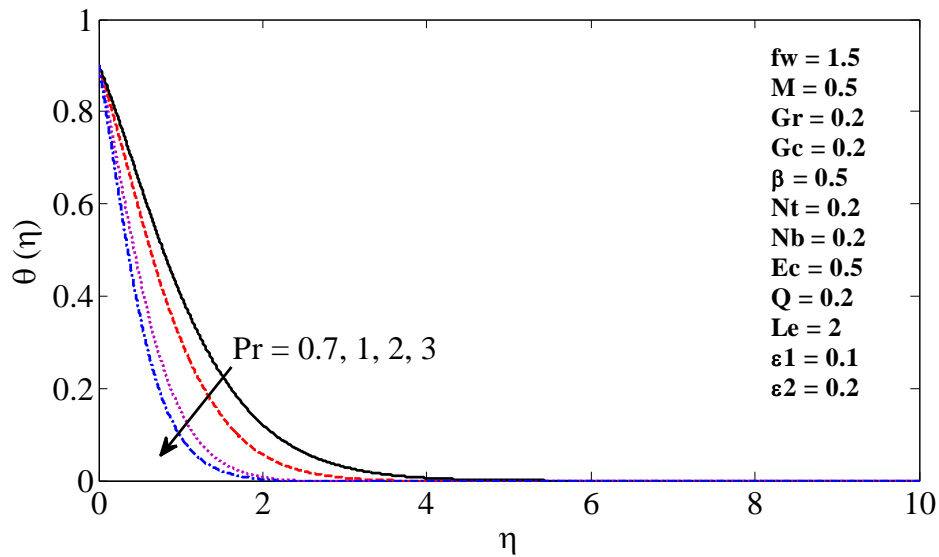


Figure 11 Temperature profiles for different values of  $Pr$

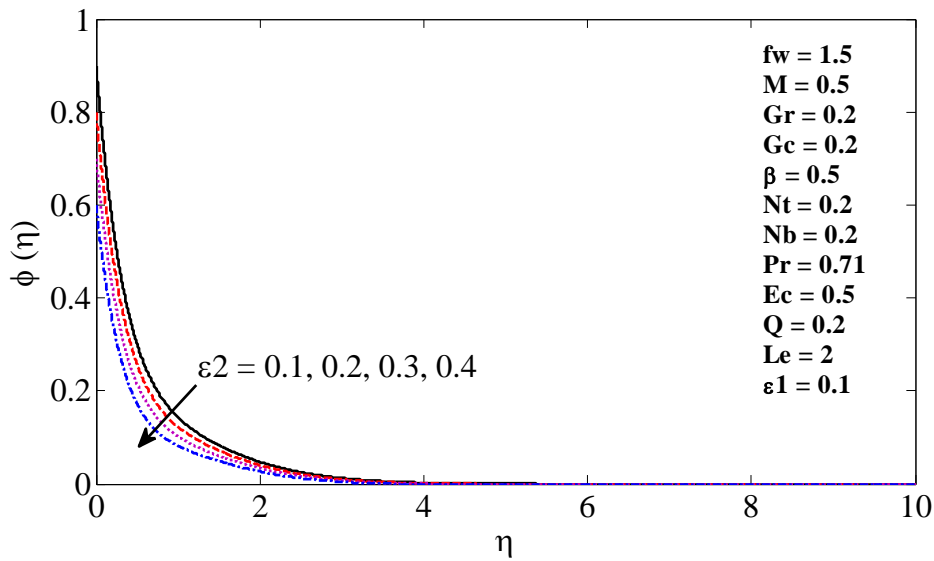


Figure 12 Concentration profiles for different values of  $\epsilon_2$

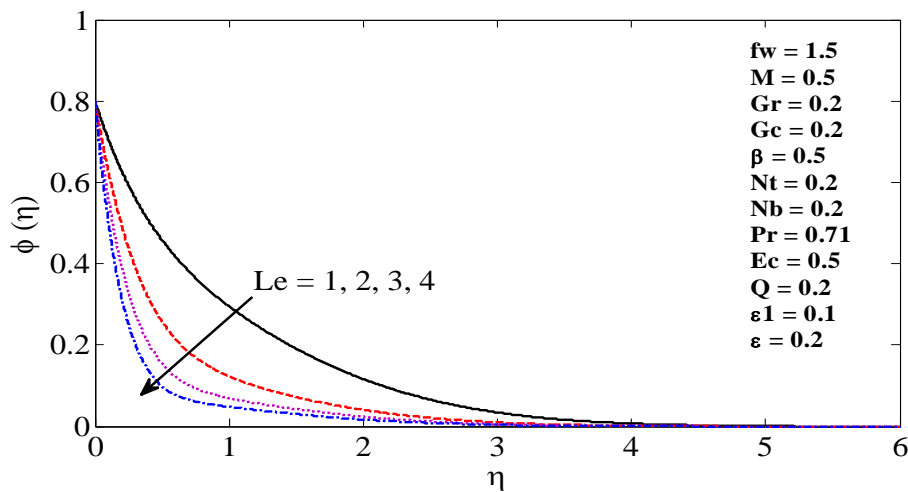


Figure 13 Concentration profiles for different values of  $Le$

**Table 2** Numerical results for local skin friction coefficient  $\left(1 + \frac{1}{\beta}\right) f''(0)$ , local Nusselt number  $-\sqrt{\frac{n+1}{2}} \theta'(0)$  and local Sherwood number  $-\sqrt{\frac{n+1}{2}} \phi'(0)$  for  $\beta, n, Gr, Gc, M, Pr, Nt, Nb$  and  $f_w$  with  $Ec = 0.5, Le = 2, Q = 0.2, \epsilon_1 = 0.1$  and  $\epsilon_2 = 0.2$ .

$\beta$	$n$	$Gr$	$Gc$	$M$	$Pr$	$Nt$	$Nb$	$f_w$	$-\left(1 + \frac{1}{\beta}\right) f''(0)$	$-\sqrt{\frac{n+1}{2}} \theta'(0)$	$-\sqrt{\frac{n+1}{2}} \phi'(0)$
0.5	2	0.2	0.2	0.5	0.71	0.2	0.2	1	2.57989	0.511266	2.405825
1	2	0.2	0.2	0.5	0.71	0.2	0.2	1	2.19806	0.520851	2.312809
1.5	2	0.2	0.2	0.5	0.71	0.2	0.2	1	2.05125	0.521417	2.273117
0.5	0	0.2	0.2	0.5	0.71	0.2	0.2	1	2.21756	0.312746	1.376311
0.5	1	0.2	0.2	0.5	0.71	0.2	0.2	1	2.49305	0.422951	1.959818
0.5	2	0.2	0.2	0.5	0.71	0.2	0.2	1	2.57989	0.511266	2.405825
0.5	3	0.2	0.2	0.5	0.71	0.2	0.2	1	2.62234	0.586843	2.781202
0.5	2	0.5	0.2	0.5	0.71	0.2	0.2	1	2.45898	0.540930	2.391204
0.5	2	1	0.2	0.5	0.71	0.2	0.2	1	2.26294	0.585471	2.369788
0.5	2	1.5	0.2	0.5	0.71	0.2	0.2	1	2.07243	0.624925	2.351547
0.5	2	0.2	0.5	0.5	0.71	0.2	0.2	1	2.52077	0.522570	2.400081
0.5	2	0.2	1	0.5	0.71	0.2	0.2	1	2.42307	0.540536	2.391028
0.5	2	0.2	1.5	0.5	0.71	0.2	0.2	1	2.32635	0.557492	2.382588
0.5	2	0.2	0.2	1	0.71	0.2	0.2	1	2.79896	0.447218	2.435701
0.5	2	0.2	0.2	2	0.71	0.2	0.2	1	3.18694	0.335016	2.492862
0.5	2	0.2	0.2	3	0.71	0.2	0.2	1	3.52798	0.237531	2.546847
0.5	2	0.2	0.2	0.5	1.0	0.2	0.2	1	2.59052	0.643284	2.302581
0.5	2	0.2	0.2	0.5	2.0	0.2	0.2	1	2.60541	0.976885	2.023731
0.5	2	0.2	0.2	0.5	3.0	0.2	0.2	1	2.61142	1.224259	1.804230
0.5	2	0.2	0.2	0.5	0.71	0.4	0.2	1	2.56393	0.475061	2.167755
0.5	2	0.2	0.2	0.5	0.71	0.6	0.2	1	2.54857	0.440846	1.987209
0.5	2	0.2	0.2	0.5	0.71	0.8	0.2	1	2.53382	0.408502	1.858898
0.5	2	0.2	0.2	0.5	0.71	0.2	0.4	1	2.58616	0.447969	2.585948
0.5	2	0.2	0.2	0.5	0.71	0.2	0.6	1	2.58754	0.391848	2.643873
0.5	2	0.2	0.2	0.5	0.71	0.2	0.8	1	2.58773	0.341021	2.671629
0.5	2	0.2	0.2	0.5	0.71	0.2	0.2	-0.5	1.75027	-0.079346	0.786018
0.5	2	0.2	0.2	0.5	0.71	0.2	0.2	-0.2	1.89661	0.018994	1.069084
0.5	2	0.2	0.2	0.5	0.71	0.2	0.2	0	1.89997	0.092032	1.272346
0.5	2	0.2	0.2	0.5	0.71	0.2	0.2	0.2	2.10715	0.169682	1.485029
0.5	2	0.2	0.2	0.5	0.71	0.2	0.2	0.5	2.27644	0.292927	1.818720

**Table 3** Numerical results for local skin friction coefficient  $\left(1 + \frac{1}{\beta}\right) f''(0)$ , local Nusselt number  $-\sqrt{\frac{n+1}{2}} \theta'(0)$  and local Sherwood number  $-\sqrt{\frac{n+1}{2}} \phi'(0)$  for  $\beta, n, Gr, Gc, M, Pr, Nt, Nb$  and  $f_w$  with  $\beta = 0.5, n = 2, Gr = 0.2, Gc = 0.2, M = 0.5, Pr = 0.71, Nt = 0.2, Nb = 0.2, f_w = 1$ .

$Ec$	$Le$	$Q$	$\epsilon_1$	$\epsilon_2$	$-\left(1 + \frac{1}{\beta}\right) f''(0)$	$-\sqrt{\frac{n+1}{2}} \theta'(0)$	$-\sqrt{\frac{n+1}{2}} \phi'(0)$
0.5	2	0.2	0.1	0.2	2.57989	0.511266	2.405825
1	2	0.2	0.1	0.2	2.56788	0.035470	2.838380
1.2	2	0.2	0.1	0.2	2.56309	-0.153815	3.010417
2	2	0.2	0.1	0.2	2.54402	-0.905089	3.692978
0.5	3	0.2	0.1	0.2	2.59042	0.505407	3.476617
0.5	4	0.2	0.1	0.2	2.59644	0.502902	4.516525
0.5	5	0.2	0.1	0.2	2.60038	0.501648	5.539850
0.5	2	-0.5	0.1	0.2	2.59171	0.898008	2.059497
0.5	2	-0.2	0.1	0.2	2.58767	0.751184	2.191875
0.5	2	0	0.1	0.2	2.58425	0.639404	2.291936
0.5	2	0.2	0.1	0.2	2.57989	0.511266	2.405825
0.5	2	0.5	0.1	0.2	2.57006	0.266173	2.621107
0.5	2	0.2	0.2	0.2	2.59373	0.495804	2.404038
0.5	2	0.2	0.25	0.2	2.60062	0.487524	2.403645
0.5	2	0.2	0.3	0.2	2.60749	0.478877	2.403588
0.5	2	0.2	0.1	0.3	2.58609	0.516708	2.198717
0.5	2	0.2	0.1	0.4	2.59229	0.522199	1.991356
0.5	2	0.2	0.1	0.5	2.59848	0.527741	1.783741

### References

- [1]. Angirasa, D., and Peterson, G. P., (1997), Natural convection heat transfer from an isothermal vertical surface to a fluid saturated thermally stratified porous medium, *Int. J. Heat Mass Transfer*, Vol.40, pp.4329–4335.
- [2]. Besthapu, P. and Bandari, S., (2015), Mixed Convection MHD Flow of a Casson Nanofluid over a Nonlinear Permeable Stretching Sheet with Viscous Dissipation, *Journal of Applied Mathematics and Physics*, Vol.3, pp.1580-1593.
- [3]. Bhattacharyya, K., Hayat T., and Alsaedi, A., (2014), Exact solution for boundary layer flow of Casson fluid over a permeable stretching/shrinking sheet, *ZAMM - Journal of Applied Mathematics and Mechanics / Zeitschrift für Angewandte Mathematik und Mechanik*, Vol.94, Issue 6, pp.522–528.
- [4]. Choi, S.U.S., (1995), Enhancing Thermal Conductivity of Fluids with Nanoparticles, *Proceedings of the ASME International, Mechanical Engineering Congress and Exposition*, Vol.66, pp.99-105.
- [5]. Eldabe N.T.M. and Salwa M.G.E., (1995), Heat Transfer of MHD Non-Newtonian Casson Fluid Flow between two Rotating Cylinders, *Journal of the Physical Society of Japan*, Vol.64,41.
- [6]. El-Dabe, N., Ghaly, A., Rizkallah, R., Ewis, K. and Al-Bareda, A., (2015), Numerical Solution of MHD Boundary Layer Flow of Non-Newtonian Casson Fluid on a Moving Wedge with Heat and Mass Transfer and Induced Magnetic Field, *Journal of Applied Mathematics and Physics*, Vol.3, pp.649-663.
- [7]. Fredrickson, A.G., (1964), *Principles and Applications of Rheology*. Prentice-Hall, Englewood Cliffs.
- [8]. Hussanan, A., Zuki Salleh, M., Tahar, R.M., Khan, I., (2014), Unsteady Boundary Layer Flow and Heat Transfer of a Casson Fluid past an Oscillating Vertical Plate with Newtonian Heating, *PLoS ONE*, Vol. 9(10): e108763. doi:10.1371/journal.pone.0108763.
- [9]. Isa, S. P. M., Arifin, N.M., and Nazar, R., (2014), Mixed convection boundary layer flow of a Casson fluid near the stagnation point over a permeable surface, *Malaysian Journal of Fundamental and Applied Sciences*, Vol.10, No.1, pp. 22-27.
- [10]. Jaluria, Y. and Gebhart, B., (1974), Stability and transition of buoyancy induced flows in a stratified medium, *J. Fluid Mech.*, Vol.66 (3), pp.593–612.
- [11]. Jaluria, Y., and Himasekhar, K., (1983), Buoyancy induced two-dimensional vertical flow in a thermally stratified environment, *Comput. Fluids*, Vol.11 (1), pp.39–49.
- [12]. Javad Alinejad and Sina Samarbakhsh (2012), Viscous Flow over Nonlinearly Stretching Sheet with Effects of Viscous Dissipation, *Journal of Applied Mathematics* Vol. 2012 (2012), Article ID 587834, 10 pages, <http://dx.doi.org/10.1155/2012/587834>
- [13]. Kalidas Das (2015), Nanofluid flow over a non-linear permeable stretching sheet with partial slip, *Journal of the Egyptian Mathematical Society*, Vol.23, Issue 2, pp.451–456.
- [14]. Khairy Zaimi, Anuar Ishak & Ioan Pop, (2014), Boundary layer flow and heat transfer over a nonlinearly permeable stretching/shrinking sheet in a nanofluid, *Scientific Reports* | 4 : 4404 | DOI: 10.1038/srep04404.
- [15]. Khan W.A., Makinde O.D., Khan Z. H., (2014), MHD boundary layer flow of a nanofluid containing gyrotactic microorganisms past a vertical plate with Navier slip, *International Journal of Heat and Mass Transfer*, Vol. 74, Pp. 285–291.
- [16]. Khan, J.A., Mustafa, M., Hayat, T., Alsaedi, A., (2014), On Three-Dimensional Flow and Heat Transfer over a Non-Linearly Stretching Sheet, Analytical and Numerical Solutions, *PLoS ONE*, Vol.9(9): e107287. doi:10.1371/journal.pone.0107287.
- [17]. Lakshmi Narayana, K., and Gangadhar, K., (2014), Magneto-nanofluid over an exponentially stretching permeable sheet with viscous dissipation, *i-manager's Journal on Mathematics*, Vol. 3, pp.17-27.
- [18]. Laxmi, T.V. and Shankar, B., (2016), Effect of Nonlinear Thermal Radiation on Boundary Layer Flow of Viscous Fluid over Nonlinear Stretching Sheet with Injection/Suction, *Journal of Applied Mathematics and Physics*, Vol.4, pp.307-319.
- [19]. Mabood F., Khan, W. A., Ismail A. I. M., (2015), MHD boundary layer flow and heat transfer of nanofluids over a nonlinear stretching sheet, *Journal of Magnetism and Magnetic Materials*, Vol. 374, Pp. 569–576
- [20]. Malik, M. Y., Naseer, M., Nadeem, S., Abdul Rehman, (2014), The boundary layer flow of Casson nanofluid over a vertical exponentially stretching cylinder, *Appl Nanosci.*, Vol.4, pp.869–873.
- [21]. Masood Khan and Hashim, (2015), Boundary layer flow and heat transfer to Carreau fluid over a nonlinear stretching sheet, *AIP Advances*, Vol.5, 107203 (2015); doi: 10.1063/1.4932627
- [22]. Masood Khan and Waqar Azeem Khan, (2016), MHD boundary layer flow of a power-law nanofluid with new mass flux condition, *AIP Advances*, Vol.6, 025211, doi: 10.1063/1.4942201.
- [23]. Muhammad A Imran, Shakila Sarwar and Muhammad Imran, (2016), Effects of slip on free convection flow of Casson fluid over an oscillating vertical plate, *Boundary Value Problems*, 2016:30, DOI 10.1186/s13661-016-0538-2
- [24]. Mustafa, M., Junaid, Khan, A., Hayat, T., Alsaedi, A., (2014), Boundary Layer Flow of Nanofluid Over a Nonlinearly Stretching Sheet With Convective Boundary Condition, *IEEE Transactions on Nanotechnology*, Vol.14 , pp. 159 – 168.
- [25]. Nadeem, S., Rizwan Ul Haq, Noreen Sher Akbar, Khan, Z.H., (2013), MHD three-dimensional Casson fluid flow past a porous linearly stretching sheet, *Alexandria Engineering Journal*, Vol.52, Issue 4 Pp. 577–582.
- [26]. Rana, P. and Bhargava, R., (2012), Flow and Heat Transfer of a Nanofluid over a Nonlinearly stretching Sheet: A Numerical Study, *Communications in Nonlinear Science and Numerical Simulation*, Vol.17, pp.212-226.
- [27]. Shampine, L. F. and Kierzenka, J. (2000), "Solving boundary value problems for ordinary differential equations in MATLAB with bvp4c," *Tutorial Notes*.
- [28]. Sohail Nadeem, Rizwan Ul Haq, Noreen Sher Akbar, (2014), MHD Three-Dimensional Boundary Layer Flow of Casson Nanofluid Past a Linearly Stretching Sheet With Convective Boundary Condition, *IEEE Transactions on Nanotechnology*, Vol.13, pp.109 – 115.
- [29]. Srinivasacharya, D., and Mendu Upendar, (2013), Effect of double stratification on MHD free convection in a micropolar fluid, *Journal of the Egyptian Mathematical Society*, Vol.21, pp.370–378.
- [30]. Swati Mukhopadhyay, (2013), Analysis of boundary layer flow over a porous nonlinearly stretching sheet with partial slip at the boundary, *Alexandria Engineering Journal*, Vol.52, Issue 4, pp. 563–569.
- [31]. Swati Mukhopadhyay, Pratiba Ranjan De, Krishnendu Bhattacharyya, Layek, G.C.,(2013), Casson fluid flow over an unsteady stretching surface, *Ain Shams Engineering Journal*, Vol. 4, Pp. 933–938.
- [32]. Wubshet Ibrahim and Bandari Shankar, (2013), MHD boundary layer flow and heat transfer of a nanofluid past a permeable stretching sheet with velocity, thermal and solutal slip boundary conditions, *Computers & Fluids*, Vol. 75, Pp.1–10.
- [33]. Yang, K. T., Novotny, J. L., and Cheng, Y. S., (1972), Laminar free convection from a non-isothermal plate immersed in a temperature stratified medium, *Int. J. Heat Mass Transfer*, Vol.15, pp.1097-1109.